Spontaneous parametric processes in optical fibers: a comparison

K. Garay-Palmett[a], M. Corona[a,b], and A.B. U'Ren[a]
[a]*Instituto de Ciencias Nucleares, Universidad Nacional Autónoma de México*
Apartado Postal 70-543, México 04510, DF, México.
[b]*Centro de Investigación Científica y de Educación Superior de Ensenada,*
Apartado Postal 2732, Ensenada B.C., 22860, México,
e-mails: karina.garay@nucleares.unam.mx; alfred.uren@nucleares.unam.mx

Recibido el 25 de enero de 2011; aceptado el 18 de marzo de 2011

We study the processes of spontaneous four-wave mixing and of third-order spontaneous parametric downconversion in optical fibers, as the basis for the implementation of photon-pair and photon-triplet sources. We present a comparative analysis of the two processes including expressions for the respective quantum states and plots of the joint spectral intensity, a discussion of phasematching characteristics, and expressions for the conversion efficiency. We have also included a comparative study based on numerical results for the conversion efficiency for the two sources, as a function of several key experimental parameters.

Keywords: Photonic nonclassical states; quantum entanglement; four-wave mixing.

Estudiamos los procesos de mezclado de cuatro ondas espontáneo y de conversión paramétrica descendente de tercer orden espontánea en fibras ópticas, como base para la implementación de fuentes de parejas y tripletes de fotones. Presentamos un análisis comparativo de los dos procesos, incluyendo expresiones para los estados cuánticos respectivos y gráficos de la intensidad espectral conjunta, una discusión de las características de empatamiento de fases, y expresiones para la eficiencia de conversión. También hemos incluído un estudio comparativo, basado en resultados numéricos, de la eficiencia de conversión para los dos procesos, en función de diferentes parámetros experimentales.

Descriptores: Estados fotónicos no clásicos; entrelazamiento cuántico; mezclado de cuatro ondas.

PACS: 42.50.-p; 03.65.Ud; 42.65.-k; 42.65.Hw

1. Introduction

Nonclassical light sources, and in particular photon-pair sources, have become essential for testing the validity of quantum mechanics [1] and for the implementation of quantum-enhanced technologies such as quantum cryptography, quantum computation and quantum communications [2]. Photon pairs can be generated through spontaneous parametric processes, in which classical electromagnetic fields illuminate optically non-linear media. Specifically, photon-pair sources are commonly based on the process of spontaneous parametric down conversion (SPDC) in second order nonlinear crystals [3]. However, in the last decade there has been a marked interest in the development of photon-pair sources based on optical fibers [4]. In fibers, the process responsible for generating photon pairs is spontaneous four-wave mixing (SFWM), which offers several significant advantages over SPDC, for example in terms of the conversion efficiency [5]. The third-order nonlinearity in optical fibers which makes SFWM possible can also lead to the generation of photon triplets through the process of third-order spontaneous parametric down conversion (TOSPDC) [6].

Recently, we have studied spontaneous parametric processes in optical fibers, including both SFWM photon-pair sources and TOSPDC photon-triplet sources. In the context of SFWM sources, we have carried out a thorough theoretical study of the spectral correlation properties between the signal and idler photons [7-9], which permits tailoring these properties to the needs of specific quantum information processing applications. In particular, our results have helped pave the way towards the experimental realization of factorable photon-pair sources [10-12], which represent an essential resource for the implementation of linear optics quantum computation (LOQC) [13]. Likewise, we have analyzed the important aspect of the attainable conversion efficiency, for the pulsed-pumps and monochromatic-pumps regimes, as well as for degenerate-pumps and non-degenerate-pumps configurations [5].

Even though a number of approaches for the generation of photon triplets have been either proposed or demonstrated [14-17], the reported conversion efficiencies have been extremely low. Recently, we have proposed a scheme for the generation of photon triplets in thin optical fibers by means of TOSPDC [6]. Our proposed technique permits the direct generation of photon triplets, without postselection, and results derived from our numerical simulations have shown that the emitted flux for our proposed source is competitive when compared to other proposals [17]. Advances in highly non-linear fiber technology are likely to enhance the emission rates attainable through our proposed technique.

In this paper, we present a comparison of the SFWM and TOSPDC processes. To this end, we assume a specific fiber with a specific pump frequency which permits the realization of both processes. We restrict our attention to SFWM involving degenerate pumps, and to TOSPDC with degenerate emitted frequencies. Our comparison includes the following aspects: i) the quantum state, leading to the joint spectrum, ii) the phasematching properties, and iii) the conversion efficiency.

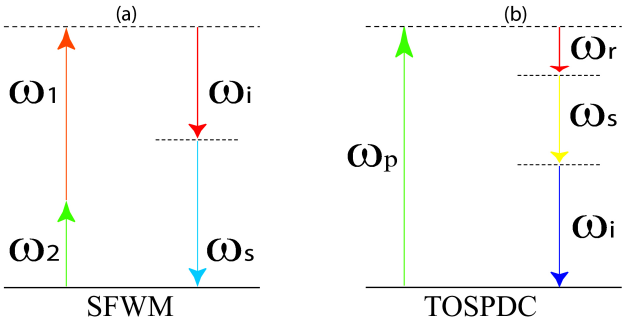

FIGURE 1. Energy level diagrams for the (a) SFWM and (b) TOSPDC processes.

2. Theory of spontaneous parametric processes in optical fibers

Non-linear processes in optical fibers originate from the third order susceptibility $\chi^{(3)}$ [18]. Photon pairs and triplets can be generated in optical fibers by means of SFWM and TOSPDC, respectively. Both of these processes, which result from four wave mixing, require the fulfilment of energy and momentum conservation between the participating fields. The current analysis focuses on configurations in which all fields are linearly polarized, parallel to the x-axis, and propagate in the same direction along the fiber, which defines the z-axis. Our work could be generalized to cross-polarized source designs.

In the case of SFWM, two photons (one from each of two pump fields) with frequencies ω_1 and ω_2 are jointly annihilated giving rise to the emission of a photon pair, where the two photons are typically referred to as signal(s) and idler(i), with frequencies ω_s and ω_i. The energy conservation relationship, thus reads $\omega_1 + \omega_2 = \omega_s + \omega_i$. In contrast, in the case of TOSPDC, a single pump photon at frequency ω_p is annihilated, giving rise to a photon triplet, where the three photons are here referred to as signal-1(r), signal-2(s) and idler(i), with emission frequencies ω_r, ω_s and ω_i. The energy conservation constraint in this case reads $\omega_p = \omega_r + \omega_s + \omega_i$. Representations of the SFWM and TOSPDC processes, in terms of the frequencies involved, are shown in Fig. 1.

2.1. Two-photon and three-photon quantum state

Following a standard perturbative approach [19] we have previously demonstrated that the SFWM two-photon state [7] and the TOSPDC three-photon state [6,20] can be written as

$$|\Psi\rangle = |0\rangle_s|0\rangle_i + \kappa\int d\omega_s \int d\omega_i F(\omega_s,\omega_i)\,|\omega_s\rangle_s\,|\omega_i\rangle_i\,, \quad (1)$$

and

$$|\Psi\rangle = |0\rangle_r|0\rangle_s|0\rangle_i + \zeta\int d\omega_r \int d\omega_s \times \int d\omega_i G(\omega_r,\omega_s,\omega_i)\,|\omega_r\rangle_r\,|\omega_s\rangle_s\,|\omega_i\rangle_i\,, \quad (2)$$

respectively, where κ and ζ are constants related to the conversion efficiency. In Eq. (1), $F(\omega_s,\omega_i)$ is the SFWM joint spectral amplitude (JSA) function and is given by [5]

$$F(\omega_s,\omega_i) = \int d\omega\,\alpha_1(\omega)\alpha_2(\omega_s+\omega_i-\omega) \times \mathrm{sinc}\left[\frac{L}{2}\Delta k(\omega,\omega_s,\omega_i)\right] e^{i\frac{L}{2}\Delta k(\omega,\omega_s,\omega_i)}, \quad (3)$$

where L is the fiber length, $\alpha_\nu(\omega)$ is the pump spectral envelope for mode $\nu = 1, 2$, and $\Delta k(\omega,\omega_s,\omega_i)$ is the phasemismatch defined as

$$\Delta k(\omega,\omega_s,\omega_i) = k_1(\omega) + k_2(\omega_s+\omega_i-\omega) - k(\omega_s) - k(\omega_i) - \Phi_{NL}, \quad (4)$$

which includes a nonlinear contribution Φ_{NL} derived from self/cross-phase modulation [7]. It can be shown that

$$\Phi_{NL} = (\gamma_1 + 2\gamma_{21} - 2\gamma_{s1} - 2\gamma_{i1})P_1 + (\gamma_2 + 2\gamma_{12} - 2\gamma_{s2} - 2\gamma_{i2})P_2, \quad (5)$$

where P_ν represents the pump peak power, and coefficients γ_1 and γ_2 result from self-phase modulation of the two pumps, and are given with $\nu = 1, 2$ by

$$\gamma_\nu = \frac{3\chi^{(3)}\omega_\nu^o}{4\epsilon_o c^2 n_\nu^2 A_{eff}^\nu}. \quad (6)$$

In Eq. 6, the refractive index $n_\nu \equiv n(\omega_\nu^o)$ and the effective area

$$A_{eff}^\nu \equiv \left[\int\int dxdy|A_\nu(x,y)|^4\right]^{-1} \quad (7)$$

(where the integral is carried out over the transverse dimensions of the fiber) are defined in terms of the carrier frequency ω_ν^o for pump-mode ν [18]. Here, functions $A_\mu(x,y)$ (with $\mu = 1, 2, s, i$) represent the transverse field distributions and are assumed to be normalized such that

$$\int\int dxdy|A_\mu(x,y)|^2 = 1. \quad (8)$$

In contrast, coefficients $\gamma_{\mu\nu}$ ($\nu = 1, 2$ and $\mu = 1, 2, s, i$) correspond to the cross-phase modulation contributions that result from the dependence of the refractive index experienced by each of the four participating fields on the pump intensities. These coefficients are given by

$$\gamma_{\mu\nu} = \frac{3\chi^{(3)}\omega_\mu^o}{4\epsilon_o c^2 n_\mu n_\nu A_{eff}^{\mu\nu}}, \quad (9)$$

where $n_{\mu,\nu} \equiv n(\omega_{\mu,\nu}^o)$ is defined in terms of the central frequency $\omega_{\mu,\nu}^o$ for each of the four participating fields, and

$$A_{eff}^{\mu\nu} \equiv \left[\int\int dxdy|A_\mu(x,y)|^2|A_\nu(x,y)|^2\right]^{-1} \quad (10)$$

is the two-mode effective overlap area (note that $A_{eff}^{\mu\nu}$=$A_{eff}^{\nu\mu}$). Although in general terms $\gamma_\nu \neq \gamma_{\mu\nu}$ it may be shown that for a SFWM interaction, the following represent valid approximations: $\gamma_1 \approx \gamma_{21} \approx \gamma_{s1} \approx \gamma_{i1}$ and $\gamma_2 \approx \gamma_{12} \approx \gamma_{s2} \approx \gamma_{i2}$. Taking these approximations into account, we arrive at the following simplified expression for Φ_{NL}

$$\Phi_{NL} = \gamma_1 P_1 + \gamma_2 P_2. \tag{11}$$

The JSA function in Eq. (3) characterizes the spectral entanglement present in the SFWM photon pairs. We have previously shown that depending on the type and degree of group velocity mismatch between the pump and the emitted photons (which can be controlled by tailoring the fiber dispersion), it becomes possible to generate two-photon states in a wide range of spectral correlation regimes [7].

We now turn our attention to the three-photon TOSPDC state given by Eq. (2), where $G(\omega_r, \omega_s, \omega_i)$ represents the TOSPDC three-photon joint spectral amplitude function. This function characterizes the entanglement present in the photon triplets and can be shown to be given by [6,20]

$$G(\omega_r, \omega_s, \omega_i) = \alpha(\omega_r + \omega_s + \omega_i)\phi(\omega_r, \omega_s, \omega_i), \tag{12}$$

where $\alpha(\omega_r + \omega_s + \omega_i)$ is the pump spectral amplitude (PSA) and $\phi(\omega_r, \omega_s, \omega_i)$ is the phasematching function (PM) which is given by

$$\begin{aligned}\phi(\omega_r, \omega_s, \omega_i) = &\,\text{sinc}\left[L\Delta k(\omega_r, \omega_s, \omega_i)/2\right] \\ &\times \exp[iL\Delta k(\omega_r, \omega_s, \omega_i)/2],\end{aligned} \tag{13}$$

written in terms of the fiber length L and the phasemismatch $\Delta k(\omega_r, \omega_s, \omega_i)$

$$\begin{aligned}\Delta k(\omega_r, \omega_s, \omega_i) = &\, k_p(\omega_r + \omega_s + \omega_i) - k_r(\omega_r) \\ &- k_s(\omega_s) - k_i(\omega_i) \\ &+ [\gamma_p - 2(\gamma_{rp} + \gamma_{sp} + \gamma_{ip})]P.\end{aligned} \tag{14}$$

In Eq. (14), the term in square brackets is the non-linear contribution to the phase mismatch, where P is the pump peak power, and γ_p and $\gamma_{\mu p}$ are the nonlinear coefficients derived from self-phase and cross-phase modulation, which are given by expressions of the same form as Eqs. (6) and (9), respectively.

The joint spectral amplitude function for TOSPDC photon-triplets [see Eq. (12)] is a clear generalization of the JSA which describes photon-pairs generated by SPDC in second order nonlinear crystals [21]. Note that while the TOSPDC JSA function is given as a simple product of functions, the SFWM JSA function [see Eq. (3)] is given by a convolution-type integral, which has an exact solution for monochromatic pump fields [8] and which likewise can be integrated analytically for Gaussian-envelope pump fields, under a linear approximation of the phase mismatch of Eq. (4) [7].

2.2. Conversion efficiency in SFWM and TOSPDC processes

A crucial aspect to consider in designing a photon-pair or photon-triplet source is the conversion efficiency, to which we devote this section. We present conversion efficiency expressions previously derived by us, for the SFWM process [5] and for the TOSPDC process [6,20], in terms of all relevant experimental parameters.

Here, we define the conversion efficiency as the ratio of the number of pairs or triplets emitted per unit time to the number of pump photons per unit time. In the case of pulsed pumps, we limit our treatment to pump fields with a Gaussian spectral envelope, which can be written in the form

$$\alpha_\nu(\omega) = \frac{2^{1/4}}{\pi^{1/4}\sqrt{\sigma}_\nu} \exp\left[-\frac{(\omega - \omega_\nu^o)^2}{\sigma_\nu^2}\right], \tag{15}$$

where ω_ν^o represents the central frequency and σ_ν defines the bandwidth (with $\nu = 1, 2$).

We showed in Ref. 5 that the SFWM photon-pair conversion efficiency can be written as

$$\begin{aligned}\eta = &\frac{2^8\hbar c^2 n_1 n_2}{(2\pi)^3 R}\frac{L^2\gamma_{fwm}^2 p_1 p_2}{\sigma_1\sigma_2(\omega_1^o p_2 + \omega_2^o p_1)} \\ &\times \int d\omega_s \int d\omega_i \, h_2(\omega_s, \omega_i)\left|f(\omega_s, \omega_i)\right|^2,\end{aligned} \tag{16}$$

in terms of a version of the joint spectral amplitude [see Eq. (3)] defined as $f(\omega_s, \omega_i) = (\pi\sigma_1\sigma_2/2)^{1/2}F(\omega_s, \omega_i)$, which does not contain factors in front of the exponential and sinc functions so that all pre-factors appear explicitly in Eq. (16), and where the function $h_2(\omega_s, \omega_i)$ is given by

$$h_2(\omega_s, \omega_i) = \frac{k_s^{(1)}\omega_s}{n_s^2}\frac{k_i^{(1)}\omega_i}{n_i^2}, \tag{17}$$

in terms of $k_\mu^{(1)} \equiv k^{(1)}(\omega_\mu)$, which represents the first frequency derivative of $k(\omega)$, and where $n_\mu \equiv n(\omega_\mu)$.

In Eq. (16), $\hbar$ is Planck's constant, c is the speed of light in vacuum, p_ν is the average pump power (for $\nu = 1, 2$), R is the pump repetition rate (we assume that two pump fields have the same repetition rate), and the parameter γ_{fwm} is the nonlinear coefficient that results from the interaction of the four participating fields and is different from the parameters γ_1 and γ_2 of Eq. (6). This parameter can be expressed as

$$\gamma_{fwm} = \frac{3\chi^{(3)}\sqrt{\omega_1^o\omega_2^o}}{4\epsilon_o c^2 n_1 n_2 A_{eff}}, \tag{18}$$

where A_{eff} is the effective interaction area among the four fields given by

$$A_{eff} = \frac{1}{\int dx \int dy A_1(x,y)A_2(x,y)A_s^*(x,y)A_i^*(x,y)}. \tag{19}$$

In the monochromatic-pumps limit, *i.e.* $\sigma_{1,2} \to 0$, it can be shown that Eq. (16) is reduced to [5]

$$\eta_{cw} = \frac{2^5\hbar c^2 n_1 n_2}{\pi}\frac{L^2\gamma_{fwm}^2 p_1 p_2}{p_1\omega_2 + p_2\omega_1} \times\int d\omega h_2(\omega, \omega_1+\omega_2-\omega)\text{sinc}^2[L\Delta k'_{cw}(\omega)/2]. \quad (20)$$

where $h_2(\omega, \omega_1+\omega_2-\omega)$ is given according to Eq. (17), and where the phase mismatch

$$\Delta k'_{cw}(\omega) = \Delta k_{cw}(\omega, \omega_1+\omega_2-\omega)$$

is written in terms of the function

$$\begin{aligned}\Delta k_{cw}(\omega_s,\omega_i) = {} & k\left[(\omega_s+\omega_i+\omega_1-\omega_2)/2\right] \\ & + k\left[(\omega_s+\omega_i-\omega_1+\omega_2)/2\right] \\ & - k(\omega_s) - k(\omega_i) - (\gamma_1 p_1 + \gamma_2 p_2). \end{aligned} \quad (21)$$

It is clear from Eqs. (16) and (20) that the SFWM conversion efficiency has a linear dependence on pump power, or alternatively the emitted flux has a quadratic dependence on this parameter. Note that although the phasemismatch has a pump-power dependence, no deviation from the linear behavior is observed for power levels considered as typical. Note that these conversion efficiency expressions are valid only in the spontaneous limit, where the pump powers are low enough to avoid generation events involving multiple pairs.

As is also clear form Eqs. (16) and (20), the conversion efficiency has a quadratic dependence on the nonlinearity coefficient γ_{fwm}, which implies that it has an inverse fourth power dependence on the transverse mode radius [18]. It can be shown that in general the double integral in Eq. (16), or the single integral in Eq. (20), scales as L^{-1}, so that taking into account the L^2 appearing as a prefactor, the conversion efficiency scales linearly with L. Likewise, it can be shown that in general the double integral in Eqs. (16) scales as σ^3, so that η in Eq. (16) has a linear dependence on the pump bandwidth.

In what follows, we focus on the conversion efficiency for the TOSPDC process. As we have shown for the pulsed-pump regime [see Eq. (15)], this efficiency can be written as [6]

$$\eta = \frac{2^{5/2}3^2c^3\hbar^2 n_p^3}{(\pi)^{5/2}\omega_p^o}\frac{L^2\gamma_{pdc}^2}{\sigma} \times\int d\omega_r\int d\omega_s\int d\omega_i h_3(\omega_r,\omega_s,\omega_i)|g(\omega_r,\omega_s,\omega_i)|^2, \quad (22)$$

which is given in terms of the function

$$h_3(\omega_r,\omega_s,\omega_i) = \frac{k_r^{(1)}\omega_r}{n_r^2}\frac{k_s^{(1)}\omega_s}{n_s^2}\frac{k_i^{(1)}\omega_i}{n_i^2}, \quad (23)$$

and the new function

$$g(\omega_r,\omega_s,\omega_i) = (\pi\sigma^2/2)^{1/4}G(\omega_r,\omega_s,\omega_i),$$

which is a version of the joint spectral amplitude $G(\omega_r,\omega_s,\omega_i)$ [see Eq. (12)], which does not contain factors in front of the exponential and sinc functions, so that all prefactors terms appear explicitly in Eq. (22).

In Eq. (22) γ_{pdc} is the nonlinear coefficient that governs the TOSPDC process, given by

$$\gamma_{pdc} = \frac{3\chi^{(3)}\omega_p^o}{4\epsilon_0 c^2 n_p^2 A_{eff}}, \quad (24)$$

with A_{eff} the effective interaction area among the four fields, which is expressed as

$$\left[\int dx\int dy A_p(x,y)A_r^*(x,y)A_s^*(x,y)A_i^*(x,y)\right]^{-1},$$

where the integral is carried out over the transverse dimensions of the fiber. Note that this nonlinear coefficient is different from parameters γ_ν and $\gamma_{\mu\nu}$ defined in Eqs. (6) and (9), respectively.

For a monochromatic pump, the conversion efficiency can be obtained by taking the limit $\sigma \to 0$ [see Eq. (22)], from which we obtain

$$\begin{aligned}\eta_{cw} = {} & \frac{2^2 3^2\hbar^2 c^3 n_p^3\gamma_{pdc}^2 L^2}{\pi^2\omega_p} \\ & \times\int d\omega_r\int d\omega_s h_3(\omega_r,\omega_s,\omega_p-\omega_r-\omega_s) \\ & \times\text{sinc}^2\left(\frac{L}{2}\Delta k_{cw}\right), \end{aligned} \quad (25)$$

where $h_3(\omega_r,\omega_s,\omega_p-\omega_r-\omega_s)$ is given according to Eq. (23), and where the phasemismatch $\Delta k_{cw}(k_r,k_s)$ [see Eq. (14)] is given by

$$\begin{aligned}\Delta k_{cw}(\omega_r,\omega_s) = {} & k_p(\omega_p) - k(\omega_r) \\ & - k(\omega_s) - k(\omega_p-\omega_r-\omega_s) \\ & + [\gamma_p - 2(\gamma_{rp}+\gamma_{sp}+\gamma_{ip})]p, \end{aligned} \quad (26)$$

where p is the average pump power. As in the case of SFWM, for TOSPDC the conversion efficiency [see Eqs. (13) and (19)] has a quadratic dependence on the nonlinear coefficient γ_{pdc}, which implies an inverse fourth power dependence on the transverse mode radius. Thus, for both processes small core radii favor a large emitted flux.

An important difference between the two processes relates to the dependence of the conversion efficiency on the pump power and bandwidth. While the TOSPDC conversion efficiency is independent of the pump power (except for the pump-power dependence of the phasemismatch, which can be neglected for typical pump-power levels), see Eqs. (22) and (25), the SFWM conversion efficiency scales linearly with the pump power. Note that in this respect the behavior for TOSPDC is identical to that observed for SPDC in second-order nonlinear crystals. Underlying this behavior is

the fact that for SFWM two pump photons are annihilated per generation event, while for TOSPDC, and for SPDC, a single pump photon is annihilated per generation event.

Likewise, it can be shown that for source designs regarded as typical, the triple integral in Eq. (22) scales linearly with the pump bandwidth σ so that the TOSPDC conversion efficiency is constant with respect to σ (within the phasematching bandwidth) [22]. Again, note that this behavior is identical to that observed for SPDC. This is to be contrasted with the linear dependence of the SFWM conversion efficiency with σ. This implies that unlike SFWM sources, for TOSPDC sources a pulsed-pump configuration does not represent an advantage vs a monochromatic-pump configuration in terms of the attainable emitted flux. In fact, the conversion efficiency for *spontaneous* four wave mixing scales with pump power and bandwidth in the same manner as for a *stimulated* process, such as second harmonic generation, based on a second order nonlinearity. This implies that (for sufficiently high pump powers) SFWM sources can be considerably brighter than both TOSPDC and SPDC sources. As a concrete illustration, in a remarkable recent SPDC experiment [23], despite extensive source optimization the observed photon-pair flux, per pump power and per unit emission bandwidth, is ~ 500 times lower compared to a representative SFWM experiment [24].

Finally, it can be shown that for source designs regarded as typical, the frequency integrals in Eqs. (22) and (25) scale as L^{-1}, so that the TOSPDC conversion efficiency exhibits a linear dependence on L as in the case of SFWM [25].

3. Phase matching properties for SFWM and TOSPDC

In this section, we describe the techniques studied by us, designed to achieve phasematching for the SFWM and TOSPDC processes in fused-silica fibers. In both cases, phasematching properties are linked to the frequency-dependence of the propagation constant $k(\omega)$ for each of the four participating fields.

On the one hand for SFWM we assume that all four fields propagate in the same transverse fiber mode, in particular in the HE_{11} fiber mode. Our treatment could be generalized to the case where the fields propagate in arbitrary transverse modes [18]. On the other hand, for TOSPDC we adopt a multi-modal phasematching strategy where the pump propagates in a different mode compared to the generated photon triplets. Note that the frequency-degenerate low-pump-power phasematching condition for TOSPDC can be written as follows: $k_p(3\omega) = 3k(\omega)$. Because of the large spectral separation between the pump and the generated photons, $k(3\omega)$ is considerably larger than $3k(\omega)$, for most common optical materials, characterized by normal dispersion. We propose to exploit the use of two different transverse modes in a thin fiber guided by air, i.e. with a fused silica core and where the cladding is the air surrounding this core. In particular, we will assume that while the TOSPDC photons all propagate in the fundamental mode of the fiber (HE_{11}), the pump mode propagates in the first excited mode (HE_{12}) [26]. We have shown that for the generation of photon-triplets at a particular degenerate frequency there is a single core radius for which the phase matching condition is fulfilled [6]. This scheme can be easily generalized to non-frequency-degenerate TOSPDC.

In order to compare the two processes, we choose a single fiber which can be used to implement both, a photon-pair SFWM source and a photon-triplet TOSPDC source. We restrict this comparison to degenerate-pumps SFWM and to TOSPDC involving frequency-degenerate triplets. As a specific design, we consider a fiber guided by air with a core radius of $r = 0.395$ μm. This core radius leads to TOSPDC phasematching involving a pump centered at $\lambda_p = 0.532$ μm and frequency-degenerate photon triplets centered at $\lambda = 1.596$ μm. Figure 2 shows graphically the phasematching properties for the two processes in terms of generation frequencies vs pump frequency [SFWM in panel (a), and TOSPDC in panel (b)]. The black curves were obtained by solving numerically, for each of the two processes, the perfect phasematching condition. We have displayed the generation frequencies obtained assuming perfect phasematching in terms of detunings: $\Delta_{s,i} = \omega_{s,i} - \omega_p$ for SFWM, and $\Delta_{r,s} = \omega_{r,s} - (\omega_p - \omega_i)/2$ for TOSPDC (ω_μ, with $\mu = r, s, i, p$, represents the frequencies for each of the participating modes). In the case of degenerate-pumps SFWM, energy conservation dictates that $\Delta_s = -\Delta_i$ so that there are only two independent frequency variables (ω_p and Δ_s) and thus Fig. 2(a) fully characterizes the relevant phasematching properties. In the case of TOSPDC, in order to obtain a similar representation of phasematching properties we fix the idler-photon frequency [to $\omega_i = 2\pi c/1.596$ μm in Fig. 2(b)], so that energy conservation dictates that $\Delta_r = -\Delta_s$. In this case, a series of plots similar to that in Fig. 2(b) each with a different value of ω_i, is required for a full characterization of the phasemathching properties.

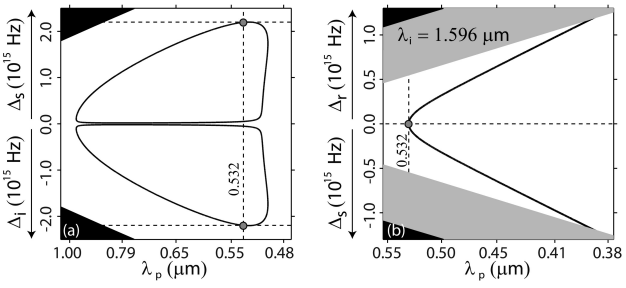

FIGURE 2. (a) Black, solid curve: perfect phasematching (Δk=0) contour for degenerate-pumps SFWM. (b) Black, solid curve: perfect phasematching (Δk=0) contour for TOSPDC with λ_i=1.596 μm. Black background: non-physical zone where energy conservation would imply that one of the generated photons has a negative frequency. Gray background: frequency zone outside of the range of validity of the dispersion relation used for fused-silica.

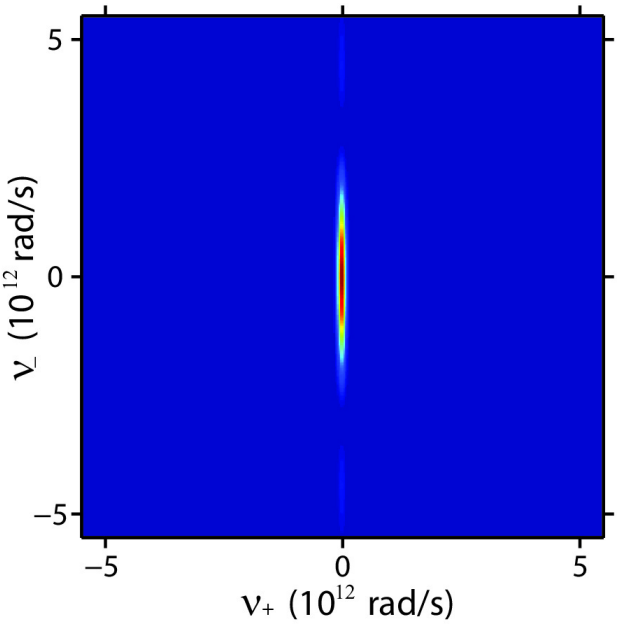

FIGURE 3. SFWM joint spectral intensity for the two-photon state, plotted as a function of frequency variables ν_+ and ν_-.

In general, for a fiber exhibiting two zero-dispersion frequencies within the spectral range of interest, the SFWM perfect phasematching contour in the space of generated vs pump frequencies is formed by two loops essentially contained between these two zero dispersion frequencies [7]; this is illustrated in Fig. 2(a). For a specific pump wavelength ω_p there may be two separate solutions for $\Delta k = 0$, leading to the inner and outer branches of the two loops. However, the inner solutions tend to be spectrally near to ω_p, with Δ_s and Δ_i strongly determined by the nonlinear contribution of the phasemismatch [see Eq. (4)], and thus pump-power dependent. This small spectral separation can lead to contamination due to spontaneous Raman scattering (which occurs within a window of $\sim$ 40 THz width towards shorter frequencies from ω_p). In order to avoid Raman contamination, we exploit the outer branches of the phasematching contour, which is comparatively less dependent on the pump power. Note that for this specific fiber, perfect phasematching occurs for pump wavelengths within a range of approximately 470nm. For the photon-triplet source proposed in this study we have chosen a pump wavelength of $\lambda_p = 0.532$ μm, that corresponds to the third harmonic of 1.596 μm, which is the selected degenerate TOSPDC frequency. For this same fiber and for the same pump wavelength, the SFWM process leads to signal and idler modes centered at 0.329 μm and 1.398 μm, respectively. In Fig. 2(a) the selected pump wavelength and the corresponding signal and idler frequencies are indicated by a black dashed line and red circle, respectively.

Unlike for the SFWM process [see Fig. 2(a)], the perfect TOSPDC phasematching contour (with ω_i kept constant) is an open curve where the vertex (red circle), corresponds to frequency-degenerate photon-triplet emission and where the selected pump frequency is indicated by a vertical

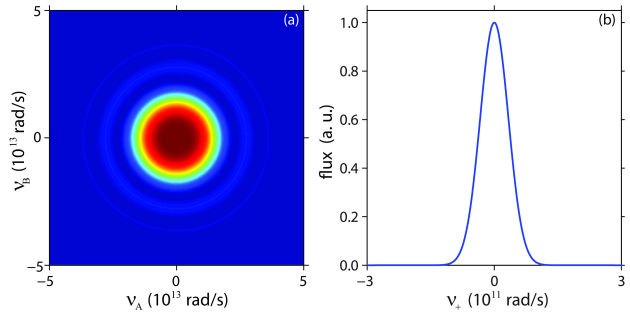

FIGURE 4. Representation of the TOSPDC joint spectral intensity obtained for the same fiber and pump parameters as in Fig. 3. (a) JSI evaluated at $\nu_+ = 0$. (b) JSI evaluated at $\nu_A = \nu_B = 0$.

black-dashed line. It can be seen that keeping ω_i constant at $\omega_p/3$, the pump can be tuned over a wide frequency range, resulting in a wide tuning range for ω_r and ω_s, away from $\omega_p/3$. It is worth mentioning that in general, the nonlinear phasemismatch contribution [see Eq. (14)] can be neglected for pump-power levels regarded as typical.

In Figs. 3 and 4 we show plots of the joint spectral intensity (JSI) function, for the SFWM and TOSPDC sources implemented with the specific fiber described above. These JSI functions are given by $|F(\omega_s, \omega_i)|^2$ and $|G(\omega_r, \omega_s, \omega_i)|^2$, respectively. If properly normalized, the JSI represents the probability distribution associated with the different emission frequencies.

A plot of the JSI shows the type and degree of spectral correlations which underlie the spectral entanglement present in the photon pairs or triplets. Typical spectral correlations imply that, for both SFWM and TOSPC, the JSI is tilted in the generated frequencies space, with narrow spectral features along specific directions. Thus, for the fiber parameters which we have assumed, the SFWM JSI exhibits a narrow width along the $\omega_s + \omega_i$ direction, and a much larger width in the perpendicular direction. In the case of TOSPDC, the JSI exhibits a narrow width along the $\omega_r + \omega_s + \omega_i$ direction and much larger widths along the perpendicular directions. This means that, for both processes, it is convenient to plot the JSI in frequency variables chosen in accordance with the correlations present.

Figure 3 shows the JSI for the SFWM source, plotted vs $\nu_+ = \frac{1}{\sqrt{2}}(\nu_s + \nu_i)$ and $\nu_- = \frac{1}{\sqrt{2}}(\nu_s - \nu_i)$, defined in terms of frequency detunings $\nu_s \equiv \omega_s - \omega_s^o$ and $\nu_i \equiv \omega_i - \omega_i^o$ where ω_s^o and ω_i^o represent signal and idler frequencies for which perfect phasematching is obtained. For this plot, we have assumed a fiber length of $L = 1$ cm and a pump bandwidth of $\sigma = 0.118$ THz (which corresponds to a Fourier-transform-limited pulse duration of 20 ps). The figure reveals that for this specific parameter combination, the signal and idler photons are spectrally anti-correlated.

Figure 4 shows a representation of the three-photon TOSPDC JSI, where we have assumed the same values for the fiber length and pump bandwidth that we used for SFWM, plotted as a function of the following frequency variables

$$\nu_+ = \frac{1}{\sqrt{3}}(\omega_r + \omega_s + \omega_i - 3\omega^o)$$
$$\nu_A = \frac{1}{2}\left(1 - \frac{1}{\sqrt{3}}\right)\omega_r + \frac{1}{2}\left(-1 - \frac{1}{\sqrt{3}}\right)\omega_s + \frac{1}{\sqrt{3}}\omega_i$$
$$\nu_B = \frac{1}{2}\left(1 + \frac{1}{\sqrt{3}}\right)\omega_r + \frac{1}{2}\left(-1 + \frac{1}{\sqrt{3}}\right)\omega_s - \frac{1}{\sqrt{3}}\omega_i. \quad (27)$$

where ω^o is defined as $\omega^o \equiv \omega_p/3$. Note that the variable ν_+ defined for TOSDPC is different to that defined for SFWM, in both cases given in terms of the sum of the generated frequencies. In Fig. 4(a), we have plotted the JSI in these new variables, evaluated at $\nu_+ = 0$, and in Fig. 4(b) we have plotted the JSI in these new variables, evaluated at $\nu_A = \nu_B = 0$. Note that the width along ν_+ is much narrower compared to the width along ν_A and ν_B, an indication of the existence of spectral correlations. The ratio of the width along ν_A or ν_B to the width along ν_+ is an indication of the strength of the correlations.

4. SFWM and TOSPDC conversion efficiency for specific source designs

In this section, we present numerical simulations of the expected conversion efficiency as a function of various experimental parameters (fiber length, pump power and pump bandwidth) for the specific SFWM and TOSPDC sources described in the previous section (see Figs. 2, 3 and 4). We include in our analysis both, the pulsed- and monochromatic-pump regimes. In order to make this comparison as useful as possible, both sources are based on the same fiber (guided by air with a core radius of $r = 0.395$ μm) and the same pump frequency ($\lambda_p = 0.532$ μm). While in the SFWM source the signal and idler modes are centered at non-degenerate frequencies ($\lambda_s = 0.329$ μm and $\lambda_i = 1.398$ μm), the TOSPDC source is frequency degenerate at $\lambda = 1.596$ μm.

For the SFWM source, the nonlinear coefficient γ_{fwm} was numerically calculated from Eq. (18) yielding a value of $\gamma_{fwm} = 629$ (kmW)$^{-1}$. The corresponding value for the TOSPDC source, numerically-calculated from Eq. (24), yields a value of $\gamma_{pdc} = 19$ (kmW)$^{-1}$. Although the two processes take place in the same fiber with the same pump frequency, the striking difference in the nonlinear coefficient results from the far superior overlap between the four participating fields in case of the SFWM source, for which the four fields propagate in the same fiber mode (HE_{11}). Taking into account the quadratic dependence of the conversion efficiency (observed for both processes) on the nonlinearity, this clearly favors a greater brightness for the SFWM source compared to the TOSPDC source.

4.1. Pump bandwidth dependence

We will first consider the conversion efficiency for the two sources described above as a function of the pump bandwidth

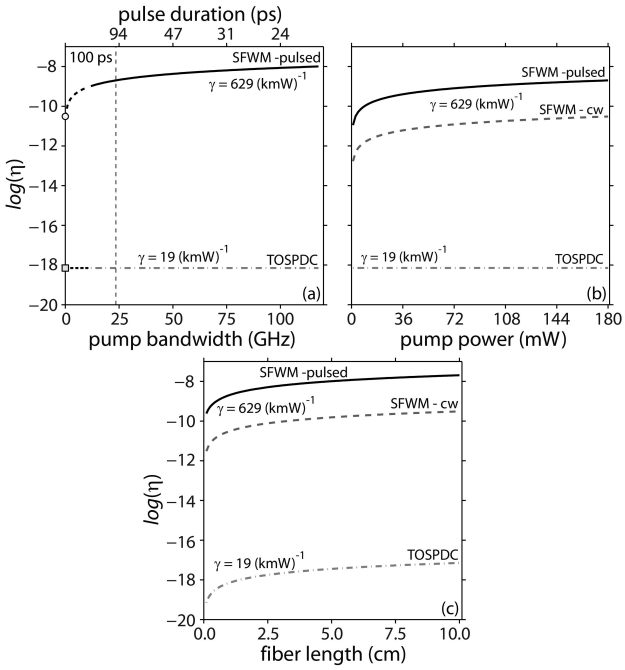

FIGURE 5. SFWM and TOSPDC conversion efficiency (in logarithmic scale) for the pulsed and monochromatic pump regimes, as a function of: (a) the pump bandwidth (the yellow circle and the green square correspond to the monochromatic-pump limit for SFWM and TOSPDC, respectively), (b) the average pump power, and (c) the fiber length.

(while maintaining the energy per pulse, or alternatively, the average power and the repetition rate constant). For this analysis, we assume a fiber length of $L = 1$ cm, a repetition rate $R = 100$ MHz and an average pump power $p = 180$ mW for both sources. Note that as σ varies, the temporal duration varies, and consequently the peak power varies too.

We evaluate the conversion efficiency from Eqs. (16) and (22) for a pump bandwidth σ range $23.5 - 117.7$ GHz (or a Fourier-transform-limited temporal duration range 20-100 ps). Numerical results for the SFWM source [obtained from Eq. (16)] and for the TOSPDC source [from Eq. (22)] are shown in Fig. 5(a) (indicated by the black solid line and the magenta dashed-dotted line, respectively). The conversion efficiency has been plotted in a logarithmic scale, considering the striking difference in order of magnitude between the efficiencies for the two processes. It can be seen that for the largest σ considered, the SFWM conversion efficiency is ten orders of magnitude greater than the TOSPDC conversion efficiency. As expected, η as given by Eq. (16), exhibits a linear dependence on the pump bandwidth (this is not graphically evident in the figure due to the logarithmic scale). The black solid line in Fig. 5(a) shows this behavior. Thus, for SFWM, the use of a pulsed pump significantly enhances the emitted flux over the level attainable for the monochromatic-pump regime. In contrast, the TOSPDC conversion efficiency remains constant over the full range of pump bandwidths considered. For this reason, in the case of TOSPDC, no difference is expected in the emitted flux, be-

tween the monochromatic- and pulsed-pump regimes (while maintaining the average pump power constant).

In the monochromatic-pump regime, evaluation of the SFWM conversion efficiency through Eq. (20) predicts a value of η_{cw}=3.05×10^{-11} [indicated by a yellow circle in Fig. 5(a)]. Likewise, we calculate the TOSPDC conversion efficiency through Eq. (25), from which we obtain η_{cw}=7.10×10^{-19}. This value is represented in Fig. 5(a) by the green square. It is graphically clear that the conversion efficiency values for $\sigma \neq 0$ [calculated from Eq. (16) and Eq. (22)] approach the corresponding values in the monochromatic-pump limit [calculated from Eq. (20) and Eq. (25)].

4.2. Pump power dependence

We now turn our attention to the pump-power dependence of the conversion efficiency for the two processes, while maintaining the pump bandwidth and other source parameters fixed. We compute the conversion efficiency as a function of the average pump power, which is varied between 1 and 180 mW. We assume a fiber length of $L = 1$ cm, a pump bandwidth of $\sigma = 23.5$ GHz (for the pulsed-pump case, corresponding to a Fourier-transform-limited temporal duration of 100 ps) and a repetition rate of $R = 100$ MHz.

Plots obtained numerically from our expressions [Eqs. (16) and (22)] are presented in Fig. 5(b), where η is expressed in a logarithmic scale. The black solid line and the magenta dashed-dotted line correspond to SFWM and TOSDPC, respectively. The SFWM conversion efficiency in the monochromatic pump limit is obtained through Eq. (20) and is indicated in Fig. 5(b) by the blue dashed line. As expected, the SFWM conversion efficiency is considerably higher in the pulsed-pump regime than in the monochromatic-pump regime. Note that TOSPDC efficiency values, obtained from Eq. (25) for the monochromatic-pump regime, are coincident with those obtained through Eq. (22) for the pulse-pump regime (see the discussion in the previous subsection).

Figure 5(b) shows that the SFWM conversion efficiency is linear with pump power (which is not graphically evident due to the logarithmic scale). Note that this linear dependence becomes quadratic for the flux vs average pump power. For the TOSPDC process, the situation is different: the conversion efficiency is constant with respect to the average pump power, while the emitted flux varies linearly with the pump power. As has already been remarked, this behavior is related to the fact that two pump photons are annihilated per generation event for SFWM, while a single pump photon is annihilated per generation event for TOSDPC. In fact, this represents one of the essential advantages of SFWM over SPDC photon-pair sources in terms of the possibility of obtaining a large emitted flux, for sufficiently high pump powers. Note that the process of TOSPDC has important similarities with the process of SPDC; in both cases, the conversion efficiency is constant with respect to the pump power and to the pump bandwidth (within the phasematching bandwidth).

At the highest average pump power considered, Eq. (16) predicts a SFWM conversion efficiency of 2.01×10^{-9}, which can be contrasted with the value obtained in the monochromatic pump limit through Eq. (20) ($\eta_{cw} = 3.05 \times 10^{-11}$). In turn, the TOSPDC conversion efficiency remains constant within the full pump-power range considered with a value of 7.11×10^{-19}, which is nine orders of magnitude lower than the conversion efficiency of SFWM with a pulsed pump.

4.3. Fiber length dependence

We now turn our attention to the fiber-length dependence of the conversion efficiency for the two processes, while maintaining other source parameters fixed. For this comparison we assume an average pump power of $p = 180$ mW and, for the pulsed case, a pump bandwidth of $\sigma = 23.5$ GHz, and a repetition rate of $R = 100$ MHz. For this study we vary the fiber length from 0.1 to 10 cm, and as before we assume a fiber radius of $r = 0.395$ μm; recent experimental work shows that it is possible to obtain a uniform-radius fiber taper of $\sim$ 445 nm radius over a length of 9 cm [27]. The results obtained by numerical evaluation of Eqs. (16) and (22) in the pulsed-pump regime are shown graphically by the black solid line for SFWM and by the magenta dash-dot line for TOSPDC. The corresponding results obtained for the monochromatic-pump regime by numerical evaluation of Eqs. (20) and (25) are presented in Fig. 5(c) by the blue dashed line for SFWM, while the curve for TOSDPC overlaps the curve calculated for the pulsed case (magenta dash-dot line). As expected, the conversion efficiency exhibits a linear dependence on the fiber length for both processes (which is not evident graphically due to the logarithmic scale). For the longest fiber considered (L=10 cm), the SFWM conversion efficiency is 2.04×10^{-8} for the pulsed-pump regime and $\eta_{cw} = 3.09 \times 10^{-10}$ for the monochromatic-pump regime, while the TOSPDC conversion efficiency is 7.13×10^{-18} (for both the pulsed- and monochromatic-pump regimes). Thus, for this specific fiber, pulsed-pumped SFWM leads to two orders of magnitude greater conversion efficiency than monochromatic-pumped SFWM, while it leads to nine orders of magnitude greater conversion efficiency than TOSDPC.

5. Conclusions

In this paper we have presented a comparative analysis of two different types of source based on spontaneous non-linear processes in optical fibers: photon-pair sources based on spontaneous four wave mixing (SFWM), and photon-triplet sources based on spontaneous third-order parametric downconversion. We have restricted our study to degenerate-pumps SFWM and to TOSPDC involving frequency-degenerate photon triplets. Likewise, we have assumed that all participating fields for each of the two types of source are co-polarized.

We have presented expressions for the quantum state of SFWM photon-pairs and TOSPDC photon-triplets, and we have discussed differences in terms of phasematching properties for the two processes. We have presented expressions for the expected source brightness for both processes, and for both: the pulsed-pump and monochromatic-pump regimes. Likewise, we have presented plots of the joint spectral intensity for both processes, which elucidate the type and degree of spectral correlations which underlie the existence of spectral entanglement in each of the two cases. We have also presented the results of a comparative numerical analysis of the attainable source brightness for each of the two sources, as a function of key experimental parameters including pump bandwidth, pump power, and fiber length.

From our study it is clear that SFWM sources can be much brighter than TOSPDC sources. This is due on the one hand to the far better degree of overlap between the four participating modes which can be attained for SFWM, for which all fields propagate in the same fiber mode (HE_{11}), unlike TOSPDC for which our phasematching strategy requires the use of two different fiber modes. On the other hand, for sufficiently high pump powers, this is due to the fact that for SFWM the conversion efficiency scales linearly with pump power and bandwidth while for TOSPDC the conversion efficiency remains constant with respect to these two parameters. Thus, unlike the case of TOSPDC, the use of short pump pulses can significantly enhance the SFWM conversion efficiency. We expect that these results will be of use for the design of the next-generation of photon-pair and photon-triplet sources for quantum-information processing applications.

Acknowledgments

This work was supported in part by CONACYT, Mexico, by DGAPA, UNAM and by FONCICYT project 94142.

1. A. Zeilinger, *Rev. Mod. Phys.* **71** (1999) 288.
2. P. Kok *et al., Rev. Mod. Phys.* **79** (2007) 135.
3. D.C. Burnham and D.L. Weinberg, *Phys. Rev. Lett.* **25** (1970) 84.
4. J.E. Sharping, M. Fiorentino, A. Coker, P. Kumar, and R.S. Windeler, *Opt. Lett.* **26** (2001) 1048.
5. K. Garay-Palmett, A.B. U'Ren, and R. Rangel-Rojo, *Phys. Rev. A* **82** (2010) 043809.
6. M. Corona, K. Garay-Palmett, and A.B. U'Ren, *Opt. Lett.* **36** (2011) 190.
7. K. Garay-Palmett *et al., Opt. Express* **15** (2007) 14870.
8. K. Garay-Palmett, A.B. U'Ren, R. Rangel-Rojo, R. Evans, and S. Camacho-Lopez, *Phys. Rev. A* **78** (2008) 043827.
9. K. Garay-Palmett, R. Rangel-Rojo, and A.B. U'Ren, *J. Mod. Opt.* **55** (2008) 3121.
10. M. Halder *et al., Opt. Express* **17** (2009) 4670.
11. O. Cohen *et al., Phys. Rev. Lett.* **102** (2009) 123603.
12. C. Söller *et al., Phys. Rev. A* **81** (2010) 031801(R).
13. E. Knill, R. Laflamme, and G.J. Milburn, *Nature* **409** (2001) 46.
14. J. Persson, T. Aichele, V. Zwiller, L. Samuelson, and O. Benson, *Phys. Rev. B* **69** (2004) 233314.
15. T.E. Keller, M.H. Rubin, and Y. Shih, *Phys. Rev. A* **57** (1998) 2076.
16. J. Rarity, and P.R. Tapster, *Phys. Rev. A* **59** (1999) R35.
17. H. Hübel *et al., Nature* **466** (2010) 601.
18. G.P. Agrawal, *Nonlinear Fiber Optics, 4th Ed.* (Elsevier, 2007).
19. L. Mandel and E. Wolf, *Optical Coherence and Quantum Optics* (Cambridge University Press, 1995).
20. M. Corona, K. Garay-Palmett, and A.B. U'Ren, submitted.
21. W.P. Grice and I.A. Walmsley, *Phys. Rev. A* **56** (1997) 1627.
22. Note that situations exist where the TOSPDC flux vs σ is not constant; *e.g.* a sufficiently long fiber implies that the resulting narrow phasematching function determines the joint amplitude function, leading to a flux which scales as σ^{-1}.
23. R. Krischek *et al., Nat. Photon* **4** (2010) 170.
24. J. Fulconis, O. Alibart, W.J. Wadsworth, and J.G. Rarity, *New J. Phys.* **9** (2007) 276.
25. Note that situations exist where the TOSPDC flux vs L is not linear; *e.g.* a sufficiently short fiber implies that the pump envelope function determines the joint amplitude function, leading to a flux which scales as L^2.
26. V. Grubsky and J. Feinberg, *Opt. Commun.* **274** (2007) 447.
27. S. Leon-Saval, T. Birks, W. Wadsworth, P. St. J. Russell, and M. Mason, *Opt. Express* **12** (2004) 2864.